Is Nubia Plate Rigid? A Geodetic Study of the Relative Motion of Different Cratonic Areas Within Africa

Mary Njoroge, Rocco Malservisi, Denis Voytenko, and Matthias Hackl

Abstract

The Nubia plate is considered to be a rigid plate and, as such, is used in the realization of International Terrestrial Reference Frame (ITRF). Geophysical and geological observations suggest that there is intraplate deformation within the Nubia plate along the Cameroon volcanic line and the Okavango rift. To test this hypothesis and to evaluate rigid plate motion, we divide the plate into three regions and calculate six Euler vectors based on available long-term GPS data.

We process the data using GIPSY-OASIS 6.2 and analyze the resulting time series for long term, annual, and semiannual signals. We calculate uncertainties for secular velocity using the Allan variance of the rate technique. We also analyze the color of the noise of each time series as a function of latitude and climatic region, and show that it is not latitude-dependent.

Although geological and geophysical studies indicate the possibility of intraplate deformation, the current Global Positioning System (GPS) network cannot identify deformation within the Nubia plate, suggesting that it is behaving as a rigid plate within uncertainty.

1 Introduction

Plate rigidity is one of the main paradigms of plate tectonics and is a fundamental assumption in the definition of a global reference frame like the ITRF (e.g. Altamimi et al. 2011). Although still far from optimal, the recent increase in GPS instrumentation within the African region allows us to better understand the applicability of the rigidity assumption to the Nubia plate.

The Nubia plate corresponds to the western and largest part of Africa. It formed from the early Miocene division of the African region along the continental East African Rift system (EARs) (Roberts et al. 2012) and is bordered by four extensional boundaries on the east, northeast, west, and south, and one compressional boundary on the northwest (Chu and Gordon 1999; Bird 2003). The continental part of the Nubia plate is composed of three large Archean cratonic regions (West Africa, Congo, and South African Kalahari) with lithospheric mantle thickness greater than 300 km (Begg et al. 2009), indicating a low degree of recent tectonic activity. The cratons are separated by old suture zones of possibly weaker lithosphere (e.g., Begg et al. 2009; Tokam 2010). The Nubia plate and its counterpart, the Somalia plate on the East side of EARs, are linked together by three microplates: Victoria, Rovuma, and Lwandle (Fig. 1), which

M. Njoroge (✉) • R. Malservisi • D. Voytenko
University of South Florida, Tampa, FL, USA
e-mail: mnjoroge@mail.usf.edu

M. Hackl
Allianz SE Reinsurance, Munich and Germany
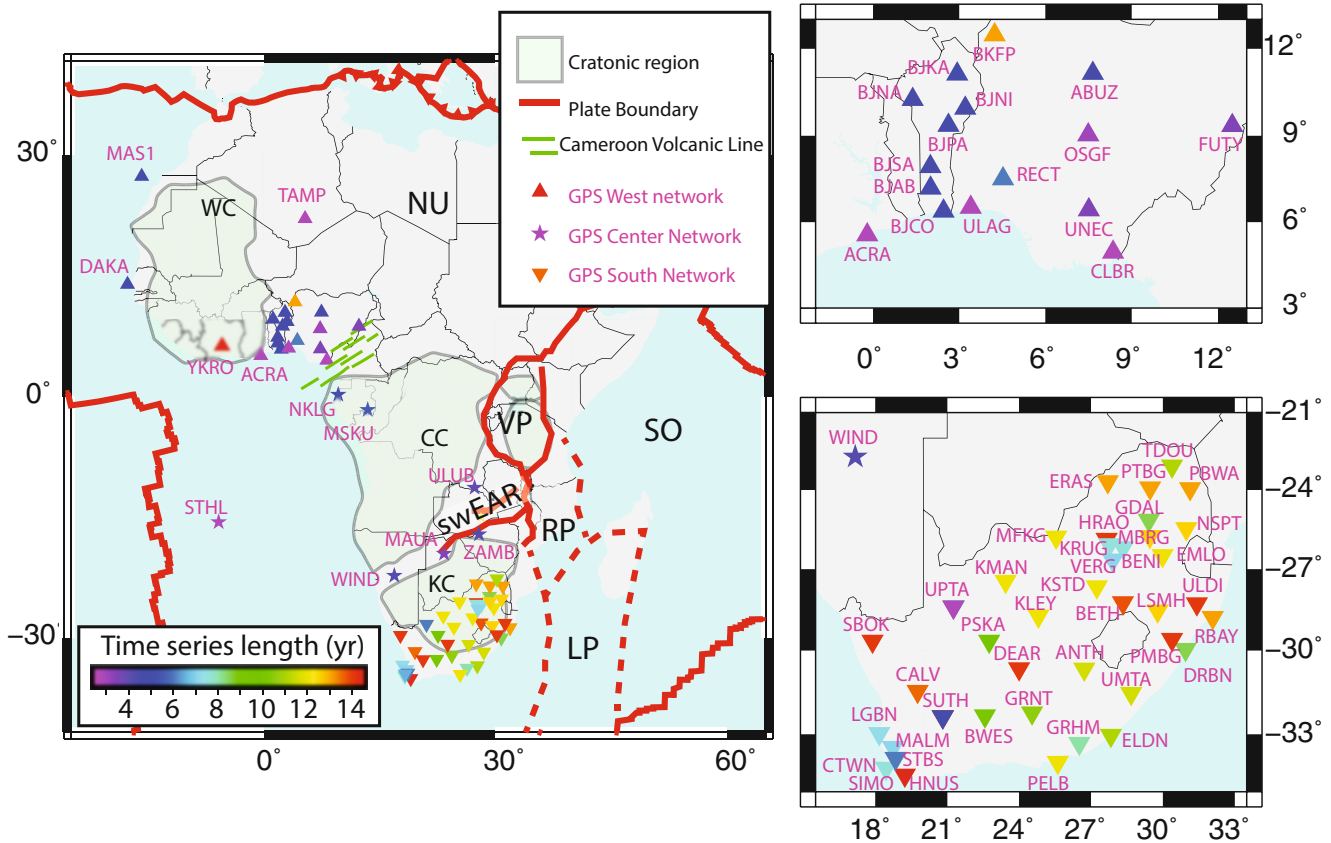
Fig. 1 Map of Africa showing the Nubia (NU) and Somalia (SO) plates and the three microplates: Victoria Plate (VP), Rovuma Plate (RP), and Lwandle Plate (LP). The swEAR indicates the South West continuation of the EARs. *Green lines* indicate the Cameroon volcanic line. *WC* indicates the West African craton, *CC* the Congo craton, and *KC* the Kalahari Craton (from Begg et al. 2009). *Red lines* show well-defined (*solid*) and assumed (*dashed*) plate boundaries (from Bird 2003 and Stamps et al. 2008). The three Nubia plate cratons (West Africa, Congo, and Kalahari) are labeled. GPS sites are color coded by time series length with a symbol indicating their regional network. *Right side* shows enlarged maps of the West (*top*) and South (*bottom*) networks

are separated by well-defined divergent boundaries (the different branches of EARs) (Hartnady 2002; Calais et al. 2006; Stamps et al. 2008; Saria et al. 2013). Plate reconstructions indicate that the Nubia plate underwent internal deformation along the suture zones during the breakup of Gondwana (e.g., Reeves and De Wit 2000; Eagles 2007; De Wit et al. 2008). Observed seismicity, geomorphology, and geophysical data suggest that the Cameroon volcanic line (CVL, the region separating West Africa and Congo cratons and a hot spot track) and the southwest propagation of the East African Rift System (swEAR) are tectonically active (e.g., Midzi et al. 1999; Modisi 2000; Hartnady 2002; Shemang and Molwalefhe 2011; Yu et al. 2015). Previous geodetic studies show that internal tectonic deformation within the Nubia plate is ≤0.6 mm/year and may be located along the swEAR (Malservisi et al. 2013; Saria et al. 2013). The uncertainties are however larger than the value itself, and the location of deformation is not well-constrained.

2   Data Acquisition and Processing

We use all of the publically available continuous GPS (cGPS) data within stable Nubia from the following archives: TRIGNET (ftp://ftp.trignet.co.za), AFREF (ftp://ftp.afrefdata.org), NIGNET (http://server.nignet.net/data), UNAVCO (ftp://data-out.unavco.org/), and CDDIS (http://cddis.nasa.gov/). To obtain a reliable velocity field, we only use sites with at least 2.5 years of data (Blewitt and Lavallée 2002; Bennett et al. 2007; Malservisi et al. 2013). The sites have also been used in previous geodetic studies, however determination of stability of monumentation is beyond the scope of this study.

We divide the sites into three main regions: South, corresponding to the Kalahari craton and South Africa (46 sites); Central, corresponding to the area between the swEAR and the CVL (7 sites); and West, including all the sites northwest

of the CVL (mainly NIGNET and AMMA sites, 21 sites) (Table S1). Although the amount of analyzed data is still far from ideal for a large plate like Nubia, the velocity field presented here shows a significant improvement in time series length (3 years longer) and plate coverage (with 84 stations having more than 2.5 years of observation) compared to previous publications by Malservisi et al. (2013) and Saria et al. (2013).

We obtain daily static positions for each site using at least 20 hours of dual frequency observations. We process the data using the GIPSY–OASIS 6.2 software (Lichten and Border 1987) and the precise point positioning (PPP) method described by Zumberge et al. (1997) using orbit and clock data provided by jet propulsion laboratory (JPL). We perform phase ambiguity resolution using the single receiver algorithm (Bertiger et al. 2010), correct for ocean loading using FES2004 (Lyard et al. 2006), and calculate tropospheric delay using Vienna Mapping Functions (Boehm et al. 2006). We then align the solutions with IGb08 (Rebischung et al. 2011) through daily seven-parameter transformations (x-files) provided by JPL.

We analyze the time series for long-term trends to compute secular velocities of each site. We also analyze each component independently and correct the time series for jumps due to known equipment replacement or co-seismic signals. We visually inspect each time series and use the MATLAB code PATV (Selesnick et al. 2012) to identify other unknown jumps. We then fit each time series component using the equation

$$x(t_i) = a + vt_i + b\,cos\,(2\pi t_i + \phi_a) \\ + c\,cos\,(4\pi t_i + \phi_s) + \sum_{j=1}^{m} d_j\,H\,(t_i - t_j) \quad (1)$$

where a is the position at reference time, v is the long-term secular velocity, b and ϕ_a are the amplitude and phase of the annual signal, c and ϕ_s are the amplitude and phase of the semiannual signal, m is the number of jumps within the time series at time t_j, d_j is the unknown amplitude of the jump, and $H\,(t_i - t_j)$ is the Heaviside function.

Following the description of Njoroge (2015) and Malservisi et al. (2015), we remove daily positions that differ by more than five times the nominal uncertainty from the time series and re-fit the data in an iterative way, until no outliers remain (generally, a single iteration is enough). We detrend the resulting clean time series to compute uncertainties. Note that applying this method to time series with large and often almost periodic gaps could be problematic. Analyzing annual or semi-annual signals in such time series affects the long-term rate much more than any estimation of velocity uncertainty. In our case, we found that the effects on the station TAMP are such that does not

allow a reliable velocity estimation thus the station TAMP is not used in our analysis.

We estimate velocity uncertainties using the Allan Variance of the rate (AVR) (Hackl et al. 2011, 2013) with a combination of white and power law noise (Malservisi et al. 2013). Although we detrend the time series by removing annual and semi-annual signals, the AVR analysis indicates the presence of a periodic signal with a period between 70 and 100 days. Although we do not conduct a full spectral analysis to identify such a period, the best fit of the AVR occurs with a periodic signal of 89 days (approximately a quarter of a year), which we add to the error model. It is possible that such period is part of higher harmonic components of the yearly seasonal signal that are not removed by the filtering of Eq. (1).

Table S1 in the supplemental material has detailed information about the GPS stations and the observed secular velocities.

3   Rigid Block Motion

We apply the Euler theorem (McKenzie and Parker 1967) to calculate the rigid motion of each region with respect to IGb08. We use methodology described by Plattner et al. (2007) and Malservisi et al. (2013) to identity stations producing the best-fitting Euler vector for each region. As described in Malservisi et al. (2013) stations with larger residuals do not move according to rigid plate motion. A part from tectonic motion, various factors such as bad monumentation or local effects (e.g. water extraction or mining) could affect the motion. Thus we decided not to use those sites for Euler vector calculation. This process identifies the subset of stations used to calculate Euler vectors describing the rigid motion of the South, Central, and West regions and their combinations (West + Central, South + Central, and full Nubia). The reduced χ^2 of the obtained Euler vectors varies from 2.58 to 7.95, and the average rate residuals range from 0.33 to 0.61 mm/year. The Euler vectors are described in Tables S2 and S3.

It is important to note that we can identify a subset of stations with a reduced $\chi^2 \sim 1$ for each region. These stations have relatively long time series (approx. 6 years for West and Central and 12 years for South), but are often unevenly distributed and may not be representative of the local rigid block motion. We also note that velocity residuals computed using the larger number of stations are randomly oriented (Figs. S1 and S2). We thus suggest that the large reduced χ^2 is probably related to underestimated uncertainties instead of departure from rigid plate behavior. For these reasons, we prefer solutions with more stations even if the reduced $\chi^2 \gg 1$.

3.1 West Region Euler Vector

Although there are 20 stations in the West region, we only use 12 to calculate the Euler vector WEST (Fig. S1). Of the two colocated stations DAKR and DAKA, we kept DAKA (Table S1). We have no physical explanation for the large residuals of BJKA, BJNA, BJNI, BKFP and ULAG. It is likely that ACRA is influenced by anthropogenic activity (oil and groundwater extraction) while high residuals at YKRO may be related to the nearby Lake Kossou (Malservisi et al. 2013) observed similar behavior at sites close to lakes in South Africa). The reduced χ^2 of the resulting Euler vector is 2.58 and the mean rate residual is 0.49 mm/year (Table S2).

3.2 Central Region Euler Vector

It's the least sampled region with only seven stations. Malservisi et al. (2013) and Saria et al. (2013) showed that MSKU and ULUB have large residuals and were not used for our calculations (Table S1). Using the remaining five stations (Fig. S1) results in a reduced χ^2 of 2.65 and rate residual of 0.33 mm/year (Euler vector CENTRAL in Table S2).

3.3 South Region Euler Vector

South Africa is the region with the densest GPS coverage. Of the co-located sites HARB, HRAC, and HRAO; SUTH, SUT1, and SUTM; and UPTA and UPTN, we kept HRAO, SUTH, and UPTA respectively (Table S1). We used 28 stations to fit the Euler vector (Fig. S1). The reduced χ^2 and average residual are 7.95 and 0.39 mm/year respectively (Euler vector SOUTH in Table S2). This region also had stations with the longest time series and hence low velocity uncertainties, explaining the higher reduced χ^2. We tested the possibility of reducing the χ^2 by using sites in the driest and most stable part of the network identified by Malservisi et al. (2013) but this resulted in no significant improvement. Note that the homogeneous velocity field in the Cape Town area that Malservisi et al. (2013) suggested was related to strain accumulation is no longer visible, indicating that it may have been an artifact associated with the length of the time series.

4 Combined Euler Vectors

4.1 West-Central Region Euler Vector

To obtain this Euler vector (WEST_C in Table S2) we eliminate three extra stations due to high residuals

(FUTY, BJBA and BJPA) from those used for the WEST and CENTRAL Euler Vectors. Using the remaining 14 stations (Fig. S2), the resulting fit for the Euler vector has a reduced χ^2 of 4.89 and mean rate residual of 0.61 mm/year.

4.2 South-Central Region Euler Vector

This region consists of stations in the South and Central regions (SOUTH_C in Table S2). We used only 33 sites which were used in computation of SOUTH and CENTRAL Euler vector to calculate SOUTH_C Euler vector (Fig. S2). The reduced χ^2 and mean rate residual are 7.27 and 0.41 mm/year respectively.

4.3 Nubia Euler Vector

To calculate the NUBIA Euler vector, we rely on 42 sites used to calculate the WEST_C and SOUTH_C Euler vectors (Fig. S2). The reduced χ^2 and mean rate residual of this Euler vector calculation are 6.79 and 0.47 mm/year respectively (Table S2).

The large reduced χ^2 of some Euler vector fits may be related to underestimated uncertainties. This may be due to the error model used in the AVR interpolation (periodic, power-law, and white noise) or an underestimation of a higher time-correlated noise component (random walk). Another possibility is that flicker noise is much stronger than the time-correlated noise components, which can only be observed with much longer time series. This is particularly true using AVR, where only ¼ of the full time series length is used to calculate the variance. In both cases, the error model predicts smaller uncertainties resulting in the large reduced χ^2.

In all Euler vector calculations, most stations have residuals <0.5 mm/year, indicating a possible upper limit for the internal deformation of the Nubia plate. The few stations with residuals >1 mm/year appear to be stations with problematic behavior, short time series, or gaps. All other stations, with residuals between 0.5 and 1.0 mm/year, are more likely be affected by local phenomena (e.g., subsidence or anthropogenic effects) rather than tectonic motion.

5 Comparison of Euler Vectors

Traditionally, Euler vectors are compared separately by plotting the position of the Euler pole (with relative error ellipses) and its rate (with relative uncertainties). Since the three components of the Euler vector are
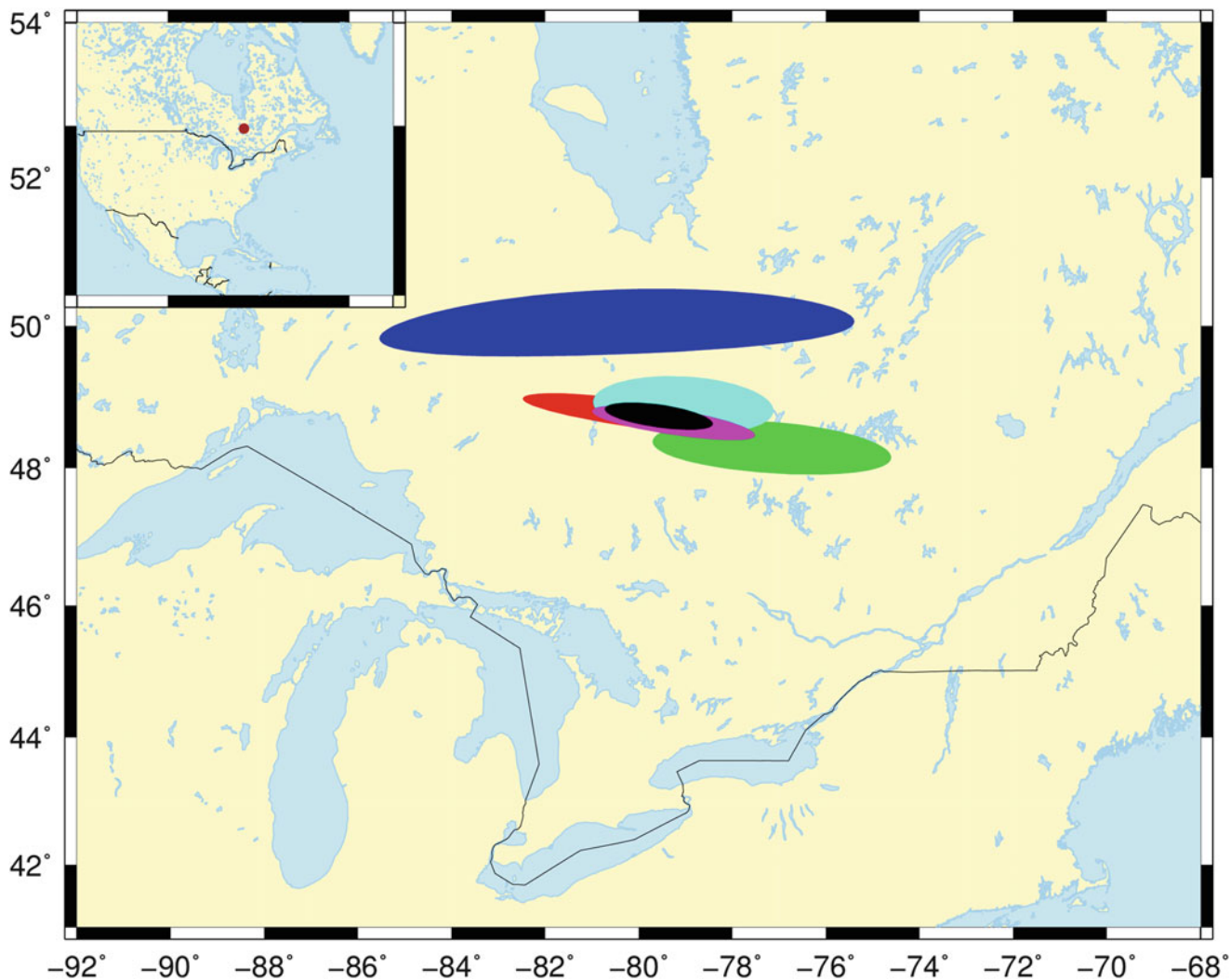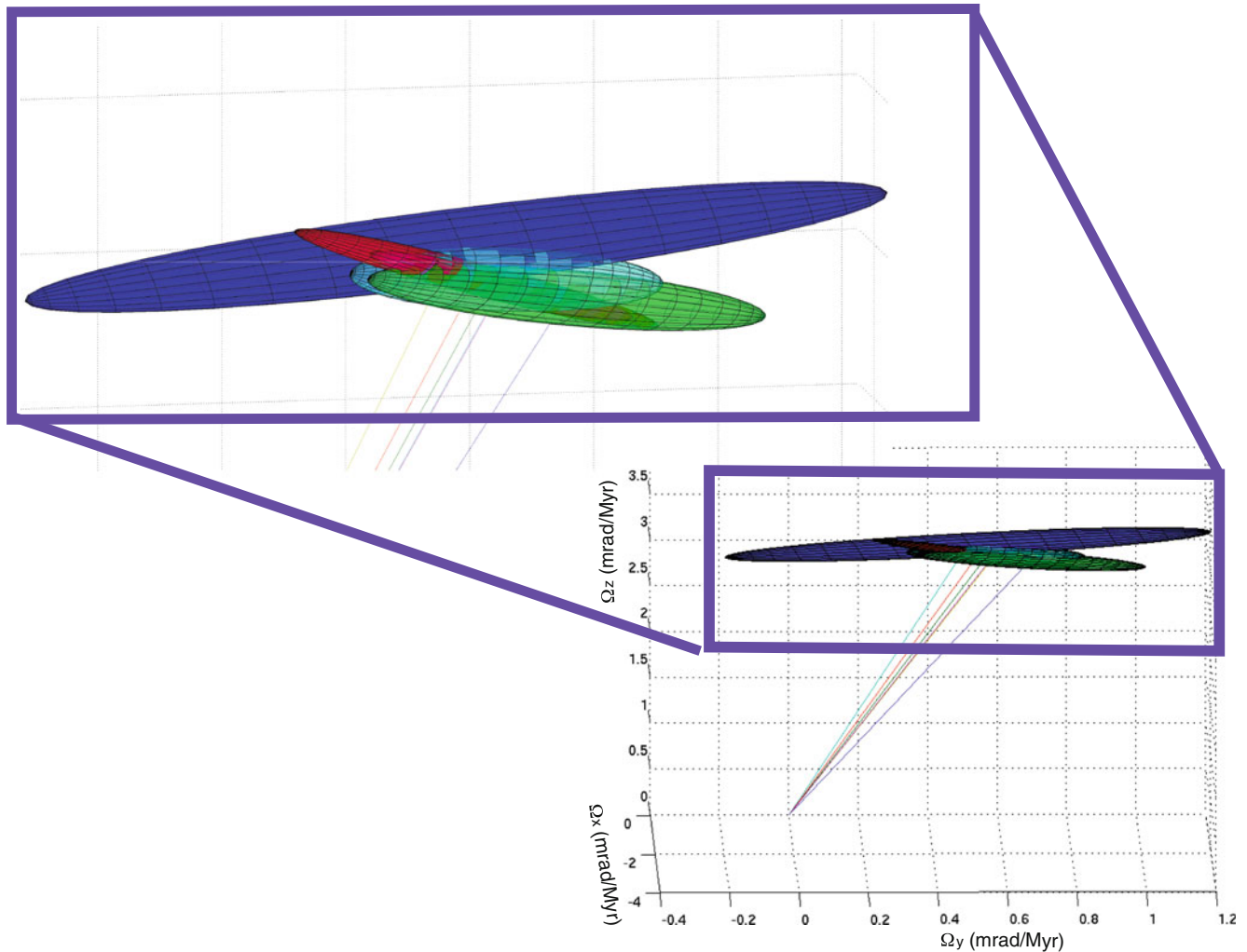
Fig. 2 Positions and 2σ error ellipses (95% confidence) of the six Euler poles: WEST (*blue*), CENTRAL (*green*), WEST_C (*cyan*), SOUTH_C (*magenta*), SOUTH (*red*), and NUBIA (*black*) in 2-dimensions, calculated with respect to the IGb08 reference frame. Within uncertainties, all of the poles except the WEST pole are compatible with each other. (The *brown circle* in the *inset* map indicates the location of the Euler poles.)

highly correlated, it is beneficial to compare the full vectors with error ellipsoids instead of ellipses. In order to make the error directly comparable, we decided to use for the 2D and 3D cases the same confidence intervals (68% and 95%) as described by Vanicek and Krakiwsky (1987). By comparing the six Euler poles calculated in this study using relative error we observe that five of them overlap at 95% confidence (Fig. 2) while four of them overlap at 68% confidence (Fig. S3). WEST Euler pole (Figs. 2 and S3) is significantly separated, suggesting that there may be relative motion between West Africa and the rest of Nubia. When comparing Euler vectors using the full covariance matrix (Fig. 3),

we observe that all ellipsoids overlap at 95% confidence, indicating that at the current level of uncertainties, we cannot rule out rigid plate behavior. The ellipsoids are also partially overlapping (Fig. S4) at 68% confidence, meaning that the likelihood of rigid plate behavior for the full Nubia plate is significant, and that with current uncertainties and network geometry, the Nubia plate moves as a rigid block with respect to IGb08. Comparing our Nubia Euler vector with those of Altamimi et al. (2007), Nocquet et al. (2006) and Stamps et al. (2008) (Figs. S5 and S6) shows that the four vectors are compatible within uncertainties when using the full covariance (Fig. S6).

Fig. 3 Error ellipsoids (95% confidence) of six Euler vectors: WEST (*blue*), CENTRAL (*green*), WEST_C (*cyan*), SOUTH_C (*magenta*), SOUTH (*red*), and NUBIA (*black*) in three dimensions, calculated with respect to the IGb08 reference frame. All Euler vector ellipsoids intersect each other. WEST has the largest ellipsoid while NUBIA and SOUTH_C are overlapped completely

6   Annual Signal Amplitude

Many periodic signals affect GPS time series (e.g., satellite orbit configuration, seasonal variation of atmospheric water content, and groundwater storage) and are usually most prominent in the vertical component (Van Dam et al. 2010; Blewitt and Lavallée 2002; Hinderer et al. 2009; Nahmani et al. 2012). Here, we analyze the variation of the annual signal (b in Eq. 1) and how it changes as function of latitude.

The annual variation of the horizontal component ranges between 0.1 and 0.2 mm and is of similar magnitude to the repeatability of the site position. The only stations with large horizontal annual amplitudes are MSKU and KSTD, which do not fit the rigid plate behavior. The amplitude of the annual signal of the vertical component varies from 0.5 to 2.5 mm, and has strong regional variation. In the Southern and driest region, the annual signals have low amplitudes, while sites within the Western region and the Congo and Zambezi basins show large amplitudes (Fig. 4). These annual amplitudes correlate with the climatic variability of the two regions (e.g., Nahmani et al. 2012 and Ramillien et al. 2014). The central part of the West region (5° N to 15° N) has amplitudes of 1.5 to 2.5 mm, and is strongly affected by the West Africa Monsoon (WAM) (Bock et al. 2008). The second largest annual signal is at MAUA, near the Okavango River delta, one the largest inland river deltas with extensive seasonal flooding (McCarthy 1993). The phases of the annual signal also agree with the observations of Nahmani et al. (2012) and Ramillien et al. (2014) and with the water cycle (Crowley et al. 2006; Ramillien et al. 2014): the peak of the annual signal for the West network is completely out of phase with the amplitude at MAUA and the other sites around the Zambezi/Congo basins (Fig. 4). This suggests that
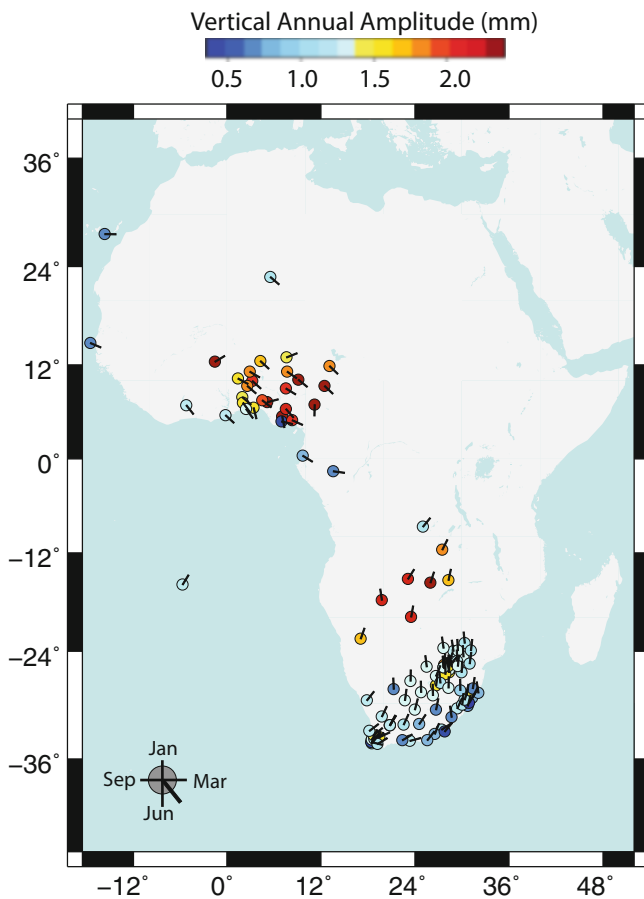
Fig. 4 Signal amplitudes of the vertical GPS component of the Nubia plate. Amplitudes vary with latitude: the South region has the smallest amplitudes while the West and Central regions have the largest amplitudes. *Lines* indicate the phase of the seasonal signal by pointing North if the peak of the signal is in January, and South if it is in June

hydrologic and atmospheric loading are probably the main sources of seasonal variation.

7 Noise Power Spectrum

GPS time series are affected by many sources of noise including GPS monument stability, antenna problems, multipath, and modeling assumptions (e.g., troposphere, ionosphere, oceanic and atmospheric loading, and orbits) (Wyatt 1989; Johnson and Agnew 1995; Langbein et al. 1995; Langbein and Johnson 1997). Some sources of noise are related to the water cycle, and we expect them to be dependent on latitude.

However, our analysis of the power spectrum of the noise component fit by the AVR white and power law model (Hackl et al. 2011), indicates that spectral characteristics do not vary with latitude. The spectral indices for all three GPS components at the sites on the Nubia plate fall between -0.6

and -1.1, with the majority clustering between -0.9 and -1.1 (essentially pure flicker noise). The small geographic variation suggests that the differences are more likely related to local effects (monument type, multipath, or human activities near the site) than to latitudinal variation. As already observed by Hackl et al. (2013), the power spectrum helps identify stations that are problematic or affected by transient behavior by having a spectral index closer to a random walk than to flicker noise.

8 Discussion and Conclusions

Despite geological and geophysical observations suggesting that there is internal deformation within the Nubia plate, our analysis shows that within our current network geometry and uncertainties, the Nubia plate behaves like a rigid block. Thus, the assumption of a rigid Nubia plate would not significantly bias a global reference frame. The Euler vectors calculated in this study indicate that the West region is the only region that may move relative to the rest of the plate. The ellipsoid corresponding to the Euler vector describing the rigid motion of this region is the only one not nested within the others. Nonetheless, it is still compatible with the other Euler vectors within 68% confidence.

Given the geophysical and geological observations of possible deformation along the CVL and swEAR, we suggest that better geometry and denser local networks are needed to identify tectonic signals in those regions.

Even within regions with a denser network like the South African Cape Town region, the GPS network is not sufficient to observe slow tectonic signals. Historically, this area has been affected by moderate to strong earthquakes (Midzi et al. 1999, 2013), but the GPS data do not show significant strain accumulation. Detailed studies accounting for local effects at each station, and a better realization of local reference, are necessary to identify such signals.

Large reduced χ^2 and the magnitude and orientation of residuals suggest that we underestimate uncertainties. Our choice of the error model (a periodic signal combined with white and power law noise) could lead to such underestimation, or we may need longer time series to better estimate the higher correlated noise. Time series are affected by both anthropogenic (e.g. mining, agricultural, water extraction, and damming) and natural (drought, water cycle, and atmospheric) signals that are quasi-periodic. These signals may affect our velocity field and uncertainty estimation because they cannot be fully corrected for using periodic signals. A detailed analysis similar to Karegar et al. (2015) could improve our ability to separate these quasi-periodic signals and to better quantify the velocity field and its uncertainties. Furthermore, a denser and better distributed GPS network is

needed for an improved understanding of intraplate deformation and associated hazards.

A.1   Electronic Supplementary Material

Below is the link to the electronic supplementary material.
[INSERT CAPTION HERE] (PDF 310 kb)
[INSERT CAPTION HERE] (PDF 187 kb)
[INSERT CAPTION HERE] (PDF 2584 kb)
[INSERT CAPTION HERE] (PDF 402 kb)
[INSERT CAPTION HERE] (PDF 2562 kb)
[INSERT CAPTION HERE] (PDF 451 kb)
[INSERT CAPTION HERE] (DOCX 24 kb)

References

Altamimi Z, Collilieux X, Legrand J, Garayt B, Boucher C (2007) ITRF2005: a new release of the international terrestrial reference frame based on time series of station positions and Earth orientation parameters. J Geophys Res 112, B09401. doi:10.1029/2007JB004949

Altamimi Z, Collilieux X, Métivier L (2011) ITRF2008: an improved solution of the international terrestrial reference frame. J Geod 85(8):457–473. doi:10.1007/s00190-011-0444-4

Begg GC et al (2009) The lithospheric architecture of Africa: seismic tomography, mantle petrology and tectonic evolution. Geosphere 5:23–50

Bennett RA, Hreinsdóttir S, Velasco MS, Fay NP (2007), GPS constraints on vertical crustal motion in the northern Basin and Range. J Geophys Res Solid Earth 34. doi:10.1029/2007GL031515

Bertiger W, Desai SD, Haines B, Harvey N, Moore AW, Owen S, Weiss JP (2010) Single receiver phase ambiguity resolution with GPS data. J Geod 84:327–337. doi:10.1007/s00190-010-0371-9

Bird P (2003) An updated digital model of plate boundaries. J Earth Sci 1027:1525–2027. doi:10.1029/2001GC000252

Blewitt G, Lavallée D (2002) Effect of annual signals on geodetic velocity. J Geophys Res. doi:10.1029/2001JB000570

Bock O et al (2008) The West African Monsoon observed by ground based GPS receivers during the AMMA project. J Geophys Res 113, D21105. doi:10.1029/2008JD010327

Boehm J, Werl B, Schuh H (2006) Troposphere mapping functions for GPS and very long baseline interferometry from European Centre for Medium-Range Weather Forecasts operational analysis data. J Geophys Res 111, B02406. doi:10.1029/2005JB003629

Calais E, Ebinger CJ, Hartnady C, Nocquet JM (2006) Kinematics of the East African Rift from GPS and earthquake slip vector data. In: Yirgu G, Ebinger CJ, Maguire PKH (eds) The Afar Volcanic province within the East African Rift system, vol 259. Geological Society London Special Publications, London, UK, pp 9–22

Chu D, Gordon R (1999) Evidence for motion between Nubia and Somalia along the Southwest Indian Ridge. Nature 398:64–66

Crowley JW, Mitrovica JX, Bailey RC, Tamisiea ME, Davis JL (2006) Land storage within the Congo Basin inferred from GRACE satellite gravity data. Geophys Res Lett 33, L19402. doi:10.1029/2006GL027070

De Wit M, Stankiewicz J, Reeves C (2008) Restoring Pan-African Brasiliano connections: more Gondwana control, less Trans-Atlantic corruption. Geol Soc 294:399–412. doi:10.1144/SP294.20

Eagles G (2007) New angles on South Atlantic opening. Geophys J Int 168:353–361

Hackl M, Malservisi R, Hugentobler U, Wonnacott R (2011) Estimation of velocity uncertainties from GPS time series: examples from the analysis of the South African TrigNet network. J Geophys Res 116, B11404. doi:10.1029/2010JB008142

Hackl M, Malservisi R, Hugentobler U, Jiang Y (2013) Velocity covariance in the presence of anisotropic time correlated noise and transient events in GPS time series. J Geodyn 72:36–45

Hartnady CJH (2002) Earthquake hazard in Africa: perspectives on the Nubia-Somalia boundary. S Afr J Sci 98:425–428

Hinderer J et al (2009) The GHYRAF (Gravity and Hydrology in Africa) experiment: description and first results. J Geodyn 48:172–181

Johnson H, Agnew DC (1995) Monument motion and measurements of crustal velocities. Geophys Res Lett 22:2905–2908

Karegar M, Dixon TH, Malservisi R (2015) A three-dimensional surface velocity for the Mississippi Delta: implications for Coastal restoration and flood potential. Geol Soc Am. doi:10.1130/G36598.1

Langbein J, Johnson H (1997) Correlated errors in geodetic time series: implications for time-dependent deformation. J Geophys Res 102:591–603

Langbein J, Dzurisin D, Marshall G, Stein R, Rundle J (1995) Shallow and peripheral volcanic sources of inflation revealed by modeling two-color geodimeter and leveling data from Long Valley Caldera, California, 1988–1992. J Geophys Res 100:12487–12495

Lichten S, Border J (1987) Strategies for high-precision global positioning system orbit determination. J Geophys Res Solid Earth 192:12751–12762. doi:10.1029/JB092iB12p12751

Lyard F, Lefevre F, Letellier T (2006) Modelling the global ocean tides: modern insights from FES2004. Ocean Dyn 56(5–6):394–415. doi:10.1007/s10236-006-0086-x

Malservisi R, Ugentobler U, Wonnacott R, Hackl M (2013) How rigid is a rigid plate? Geodetic constraint from the TrigNet CGPS network, South Africa. Geophys J Int 192:918–928. doi:10.1093/gji/ggs081

Malservisi R, Schwartz SY, Voss N, Protti M, Gonzales V, Dixon TH, Jiang Y, Newman AV, Richardson JA, Walter JI, Voytenko D (2015) Multiscale postseismic behavior on a megathrust: the 2012 Nicoya earthquake, Costa Rica. Geochem Geophys Geosyst 16. doi:10.1002/2015GC005794

McCarthy TS (1993) The great inland deltas of Africa. J Afr Earth Sci 17(3):275–291

McKenzie D, Parker R (1967) The North Pacific: an example of tectonics on a sphere. Nature 216:1276–1280

Midzi V, Hlatywayo D, Chapola L, Kebede F, Atakan K, Lombe D, Turyomurugyendo G, Tugume F (1999) Seismic hazard assessment in Eastern and Southern Africa. Ann Geofis 42:1067–1083

Midzi J, Bommer J, Strasser FO, Albini P, Zulu BS, Prasad K, Flint NS (2013) An intensity database for earthquakes in South Africa from 1912 to 2011. J Seismol 17(4):1183–1205

Modisi M (2000) Fault system of the southeastern boundary of the Okavango Rift, Botswana. J Afr Earth Sci 30:569–578

Nahmani S, Bock O, Bouin M, Santamaría-Gómez A, Boy J, Collilieux X, Métivier L, Panet I, Genthon P, de Linage C, Wöppelmann G (2012) Hydrological deformation induced by the West African Monsoon: comparison of GPS, GRACE and loading models. J Geophys Res 117:b05409. doi:10.1029/2011jb009102

Njoroge M (2015) Is Nubia plate rigid? A geodetic study of the relative motion of different cratonic areas within Africa. Master's thesis, University of South Florida

Nocquet JM, Willis P, Garcia S (2006) Plate kinematics of Nubia-Somalia using a combined DORIS and GPS solution. J Geod 80:591–607

Plattner C, Malservisi R, Dixon TH, LaFemina P, Sella GF, Fletcher J, Suarez-Vidal F (2007) New constraints on relative motion between the Pacific Plate and Baja California microplate (Mexico) from GPS measurements. Geophys J Int. doi:10.1111/j.1365-246X.2007.03494.x

Ramillien G, Frappart F, Seoane L (2014) Application of the regional water mass variations from GRACE satellite gravimetry to large scale water management in Africa. Remote Sens 6:7379–7405. doi:10.3390/rs6087379

Rebischung P, Griffiths J, Ray J, Schmid R, Collilieux X, Garayt B (2011) IGS08: the IGS realization of ITRF2008. GPS Solution 16:483–494. doi:10.1007/s10291-011-0248-2

Reeves C, De Wit M (2000) Making ends meet in Gondwana: retracting the transforms of the Indian Ocean and reconnecting continental shear zones. Terra Nova 12:272–280

Roberts EM, Stevens NJ, O'Connor PM, Dirks PHGM, Gottfried MD, Clyde WC, Armstrong RA, Kemp AIS, Hemming S (2012) Initiation of the Western branch of the East African Rift coeval with the Eastern branch. Nat Geosci 5(4): 289–294. doi:10.1038/ngeo1432

Saria E, Calais E, Altamimi Z, Willis P, Farah H (2013) A new velocity field for Africa from combined GPS and DORIS space geodetic solutions: contribution to the definition of the African reference frame (AFREF). J Geophys Res Solid Earth 118:1677–1697. doi:10.1002/jgrb.50137

Selesnick IW, Arnold S, Dantham VR (2012) Polynomial smoothing of time series with additive step discontinuities. IEEE Trans Signal Process 60(12):6305–6318

Shemang E, Molwalefhe L (2011) Geomorphic landforms and tectonism along the eastern margin of the Okavango Rift Zone, Northwestern Botswana, as deduced from geophysical data. In: Sharkov E (ed) New frontiers in tectonics research, general problems, sedimentary basins, and island arcs. Intechopen, Rijeka, pp 169–182

Stamps DS, Calais E, Saria E, Hartnady C, Nocquet JM, Ebinger C, Fernandez R (2008) A kinematic model for the East African Rift. Geophys Res Lett 35:L05304. doi:10.1029/2007GL032781

Tokam KAP (2010) Crustal structure beneath Cameroon (West Africa) deduced from the joint inversion of Rayleigh wave group velocities and receiver functions. PhD thesis, University of Yaoundé

van Dam T, Altamimi Z, Collilieux X, Ray J (2010) Topographically induced height errors in predicted atmospheric loading effects. J Geophys Res 115, B07415. doi:10.1029/2009JB006810

Vanicek P, Krakiwsky E (1987) Geodesy: the concepts, 2nd edn. Elsevier, Amsterdam

Wyatt F (1989) Displacements of surface monuments: vertical motion. J Geophys Res 94:1655–1664

Yu Y, Gao SS, Moidaki M, Reed CA, Liu KH (2015) Seismic anisotropy beneath the incipient Okavango rift: implications for rifting initiation. Earth Planet Sci Lett 430:1–8. doi:10.1016/j.epsl.2015.08.009

Zumberge JF, Heflin M, Jefferson D, Watkins M, Webb F (1997) Precise point positioning for the efficient and robust analysis of GPS data from large networks. J Geophys Res Solid Earth. doi:10.1029/96JB03860

Part IV

Celestial to Terrestrial Frame Transformations